Dynamic Lift Coefficients for Spade Rudders on Yachts

Paul H. Miller, United States Naval Academy, Annapolis, MD

ABSTRACT

The loss of a rudder is a dangerous situation for any vessel, and with the increasingly higher aspect ratios in current sailing yacht rudder designs, a better understanding of the forces on a rudder are required. While many failures have been caused by impacts with objects, a large number have failed due to underestimation of sailing loads. While larger aspect ratios increase the lift-to-drag ratio, they also increase the bending moment about the rudder's root. Combined with thinner airfoil sections to reduce drag, modern rudders are highly stressed. Traditional design methods normally assume that the maximum lift coefficient is constant for all aspect ratios. This project combined computational fluid dynamics (CFD), finite element analysis (FEA) and the tank testing of a 1/5-scale yacht to determine suitable design lift coefficients for spade rudders of cruising and racing yachts. Two rudders of different aspect ratios were tested at various speeds, heel angles and wave conditions in the tank at the Naval Surface Warfare Center – Carderock Division. The rudders were equipped with strain gauges to determine the strains at various positions along the stock and blade. The strain profile was compared against FEA results that used a CFD prediction of the pressure profile. Through back-calculation the lift coefficients in stillwater and waves were derived. The results indicated that these lift coefficients are not constant.

NOTATION

A	Projected surface area of the rudder (in^2)
ABS	American Bureau of Shipping
Cm	Mean Chord length (in)
CFD	Computational Fluid Dynamics
C_L	Non-dimensional rudder lift coefficient
C_l	Non-dimensional section lift coefficient
E	Elastic Modulus (lb/in^2)
FEA	Finite Elelment Analysis
F_L	Lift Force (lb)
I	Moment of Inertia (in^4)
IACC	International America's Cup Class
M	Bending Moment (in-lb)
S	Rudder span (in)
SLR	Speed/length ratio
T	Torque (in-lb)
ρ	Density of water ($lb\text{-}sec^2/ft^4$)
V	Vessel speed (ft/sec)
VPP	Velocity Prediction Program

	Form Approved OMB No. 0704-0188
Report Documentation Page	

1. REPORT DATE **MAR 2007**	2. REPORT TYPE	3. DATES COVERED **00-00-2007 to 00-00-2007**
4. TITLE AND SUBTITLE **Dynamic Lift Coefficients for Spade Rudders on Yachts**		5a. CONTRACT NUMBER
		5b. GRANT NUMBER
		5c. PROGRAM ELEMENT NUMBER
6. AUTHOR(S)		5d. PROJECT NUMBER
		5e. TASK NUMBER
		5f. WORK UNIT NUMBER
7. PERFORMING ORGANIZATION NAME(S) AND ADDRESS(ES) **United States Naval Academy,Annapolis,MD,21402**		8. PERFORMING ORGANIZATION REPORT NUMBER
9. SPONSORING/MONITORING AGENCY NAME(S) AND ADDRESS(ES)		10. SPONSOR/MONITOR'S ACRONYM(S)
		11. SPONSOR/MONITOR'S REPORT NUMBER(S)

12. DISTRIBUTION/AVAILABILITY STATEMENT
Approved for public release; distribution unlimited

13. SUPPLEMENTARY NOTES

14. ABSTRACT
The loss of a rudder is a dangerous situation for any vessel, and with the increasingly higher aspect ratios in current sailing yacht rudder designs, a better understanding of the forces on a rudder are required. While many failures have been caused by impacts with objects, a large number have failed due to underestimation of sailing loads. While larger aspect ratios increase the lift-to-drag ratio, they also increase the bending moment about the rudder?s root. Combined with thinner airfoil sections to reduce drag, modern rudders are highly stressed. Traditional design methods normally assume that the maximum lift coefficient is constant for all aspect ratios. This project combined computational fluid dynamics (CFD), finite element analysis (FEA) and the tank testing of a 1/5-scale yacht to determine suitable design lift coefficients for spade rudders of cruising and racing yachts. Two rudders of different aspect ratios were tested at various speeds, heel angles and wave conditions in the tank at the Naval Surface Warfare Center ? Carderock Division. The rudders were equipped with strain gauges to determine the strains at various positions along the stock and blade. The strain profile was compared against FEA results that used a CFD prediction of the pressure profile. Through back-calculation the lift coefficients in stillwater and waves were derived. The results indicated that these lift coefficients are not constant.

15. SUBJECT TERMS

16. SECURITY CLASSIFICATION OF:			17. LIMITATION OF ABSTRACT	18. NUMBER OF PAGES	19a. NAME OF RESPONSIBLE PERSON
a. REPORT **unclassified**	b. ABSTRACT **unclassified**	c. THIS PAGE **unclassified**	**Same as Report (SAR)**	**10**	

INTRODUCTION

The ability to control the direction a vessel moves is critical to the safety of that vessel. For most vessels, directional control is achieved through the use of a rudder located near the vessel's stern. The rudder provides the necessary yaw moment to either cause the vessel to deviate from a straight course or to return the vessel to the proper course. On a sailing vessel the rudder may also serve as a lifting foil counteracting leeway. If the vessel is balanced such that the rudder carries significant side force while the vessel is on a constant heading, the loss of the rudder may mean that the vessel will be nearly uncontrollable by use of the sails alone. In addition, a rudder failure may mean a significant breach to watertight integrity of the vessel. The loss of the IACC Yacht USA 77 in 2003 was directly related to the rudder's failure which led to downflooding through the rudder shaft hole.

As with most components on a racing yacht, designers strive to maximize performance. In rudder design this includes minimizing weight and improving its hydrodynamic characteristics. To reduce weight, designers look to minimize the rudder and stock size and maximize the specific material strength and stiffness (i.e. strength or stiffness divided by the material's density). To improve hydrodynamic performance a designer will increase the aspect ratio, decrease the surface area, and modify the section thickness and shape.

From a structural analysis perspective, the rudder system, due to its high consequence of failure, must be designed with a low probability of failure. As composites generally have higher uncertainties in their strengths and less ductile failure characteristics than metals, to maintain an adequate safety margin, designers must lower the other uncertainties in the system (Miller, 1994). As most marine systems have large uncertainties in load determination (Bea, 1993), one area that may yield further improvement in rudder design is an analysis of the maximum force that a rudder may develop.

Rudders fail due to numerous causes. Groundings, collisions with large floating objects and construction errors are common. Fatigue is also an issue. Cruising and offshore racing yachts must consider the first two issues. Good quality control will address the third cause. Fatigue is more difficult to address as it is load cycle and material property dependent. Low cycle fatigue, which is dependent on a relatively few (less than 1,000 cycles), large value loadings, is particularly important to quantify. As the rudder load is constantly changing due to helm input and wave action, understanding the maximum dynamic loads is important. The maximum lift coefficient occurs when the rudder is on the verge of stall, which is typically when the rudder has been quickly turned 15-30 degrees and the vessel is rapidly bearing away. This project studied the issue by back calculating the maximum rudder loads, and their respective design coefficients of two representative rudder designs of modern sail boats.

APPROACH

This project's goal was to determine the maximum dynamic lift coefficients for two rudders of different aspect ratios at two different speeds and to compare them to industry standards. The rudders were tested on a 1:5 scale model and include dynamic effects from waves and rudder movement. The rudder deflections were recorded by strain gauges. By correlating these strains against static measurements and predicted pressure distributions generated by CFD analyses of the same conditions, FEA could be used to determine the average lift coefficient.

The theoretical background begins with an understanding of the structural configuration for the rudder. While rudders have been designed to be supported by the keel or a skeg, the most popular current configuration has the rudder cantilevered off the hull. The rudder's sole attachment to the hull is through the rudder shaft. Commonly called a spade rudder, this structural arrangement leads to large loads at the lower rudder bearing. Figure 1 shows the FEA model of one of the two spade rudders used in this project.
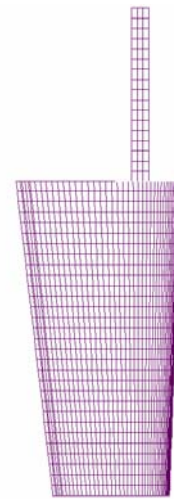

Figure 1: FEA Model of Low Aspect Ratio Spade Rudder

As the rudder acts as a lifting surface, the loads are determined from the hydrodynamic pressures generated on the rudder surface. The integration of these pressures gives the total force. While this project used a CFD prediction of the pressure distribution to get the highest accuracy, a common simplification is to assume that the force acts through the geometric centroid of the planform, which is often called the center of effort. As this centroid is located some distance from the rudder stock, a moment is generated. Because the centroid is not usually in line with the stock, a torque is also present.

To calculate the force, Bernoulli's lift equation is used:

$$F_L = \tfrac{1}{2} \rho V^2 A C_L \quad (1)$$

where F_L is the lift force. As the density of water, ρ, and the rudder's projected planform area, A, are readily determined, the two big uncertainties are the water velocity over the rudder, V, and the non-dimensional lift coefficient, C_L. When C_L is maximized at the point of stall, the maximum force is developed.

A common simplification is to assume the water velocity is equal to the vessel's speed, and for design purposes to assume that this speed is equal to the vessel's maximum speed, which can be predicted from a VPP. CFD studies have shown however that even on a straight course in flat water, the actual velocity is often less near the rudder due to the increasing dynamic pressure near the stern (Silverberg, 2003). While this lowers the velocity, a rapid turn, combined with pitch and heave, may increase the velocity during a short transient time period. As the focus of this project was to determine a suitable maximum C_L for design purposes, the common simplification was used that the velocity over the rudder was assumed to equal the vessel's speed. It is recognized however, that perhaps a more valid but computationally more difficult approach for design purposes would be to assume that C_L has a lower maximum that could be determined from constant velocity tests in a wind tunnel, and that the maximum apparent relative speed of the rudder through the water could be determined from the vessel's speed, wake, waves and vessel angular velocity.

With the assumptions that V is the vessel's speed and that the pressure distribution is relatively uniform, then the bending moment, M, and torque, T, distributions on the rudder and shaft look like Figure 2 for the rudder from Figure 1.

The maximum bending moment and torque are:

$$\begin{aligned} M_{\max} &= F_L \cdot d_v \\ T_{\max} &= F_L \cdot d_h \end{aligned} \quad (2)$$

where d_v is the vertical distance from the center of the lower rudder bearing to the centroid, and d_h is the horizontal distance from the shaft axis to the centroid.
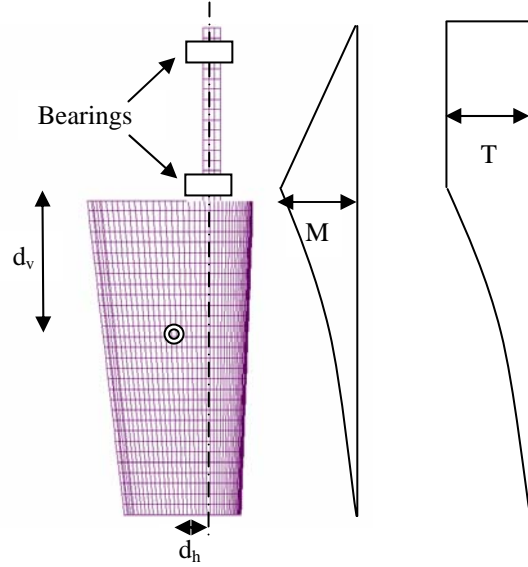

Figure 2: Moment and torque distributions for a typical spade rudder

To determine the bending stress, σ, and strain, ε, in a stock made of an isotropic material, the designer can use the relationships,

$$\sigma = \frac{F_L d_v r}{I} \quad (3)$$

$$\varepsilon = \frac{\sigma}{E} \quad (4)$$

where I is the moment of inertia of the stock, r is the stock's radius and E is the stock material's elastic modulus.

This project worked from Equation 4 backwards to find C_L from Equation 1. The strains were measured by resistance strain gauges, which combined with the known material properties, geometries and model speed in the towing tank, gave us the peak C_L for each rudder.

ABS APPROACH

The approach used in this project purposely was similar to that used by ABS (ABS 1994/1997) in their Guide for Building and Classing Offshore Racing Yachts. Section 9 of the reference lays out a method to design the rudder stock and other components. In their approach C_L is a constant 1.5 for rudders with aspect ratios between two and six and a thickness ratio greater than 6%. It is not clear whether the C_L includes an additional factor of safety, or it is entirely included in the allowable material properties, where the design allowable stress for metals is determined from either the ultimate stress divided by 2.33 or the yield stress divided by 1.33, whichever is less.

LIFT COEFFICIENTS

While the approach seems simple enough, the number of variables inherent in airfoil design make an absolute study of the dynamic effects on a sailboat rudder nearly impossible to quantify with certainty. Even taking the important assumption that the airfoil is symmetric does not significantly simplify the problem. Other studies have researched the impact of aspect ratio, leading edge shape, surface roughness and laminar to turbulent transition in the boundary area, and their impact on the maximum lift coefficient. The question remains however, "what is a reasonable maximum in practice?"

A distinction must be made between the rudder's lift coefficient, C_L, as used in Equation 1, and the local section lift coefficient, C_l. The section lift coefficient describes a 2-D lift profile, as if the wing were infinite in length. As tip vortices, root turbulence and a non-uniform spanwise flow pattern will reduce the pressure differential between the high and low pressure sides, a finite aspect ratio foil will necessarily have a C_L that is lower than the maximum C_l. Figure 3, (which is Figure 1.13 from "Aero-Hydrodynamics of Sailing" (Marchaj, 1979)) shows that C_{Lmax} for an airfoil with an aspect ratio of six is approximately 1.53, which is close to the ABS value.
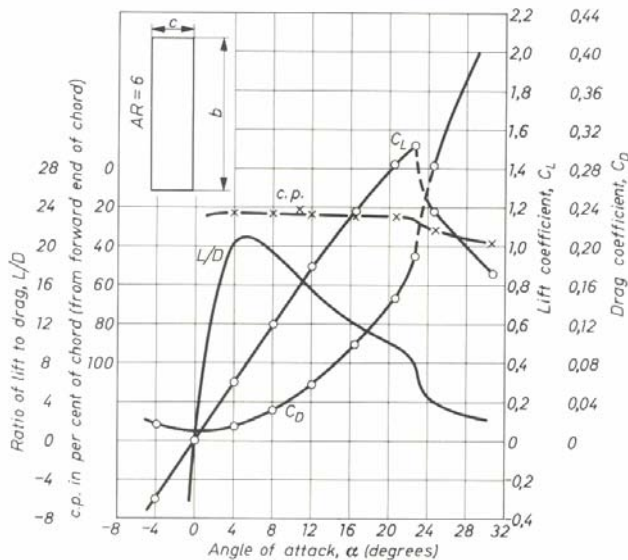

Figure 3: Airfoil characteristics for a NACA 0015 section at Re = 3.2 x 10^6.

The airfoil in Figure 3 was tested with a polished surface, which is common in well prepared, dry-sailed boats, but is unlikely in boats with bottom paint. Figure 4 (Abbott, 1959) shows the significant drop in C_{lmax} for a similar airfoil between a polished surface and a surface with a standard roughness. Roughness is particularly detrimental at the leading edge, with a drop of 24% in max C_l for a thin strip of fine sand on the leading edge. Located further back at 20% of the chord, the same thin sand strip

lowered the C_{lmax} by 10% (Abbott, 1959). To avoid issues of laminar separation, for this project the rudders were smooth but with sand strips located 10% of the chord length to help with transition from laminar to turbulent flow. From the above study it appears the strips may reduce the C_{lmax} about 15%. On the other hand, a study using Hama strips as a trip device on a similar section and aspect ratio in a tow tank indicated that although the slope of the lift curve was lower, the C_{Lmax} was perhaps 20% higher (Lewandowski, 1989).

The final question that the literature might answer is what has been done to look at rapidly changing incoming flow, where it is possible that the C_{lmax} might increase? Unfortunately, not much is available for ship rudders. In aerodynamic studies, the impact of gusts causing increased velocity are common, however are not applicable to ship rudders. Data on small angle of attack changes at constant velocity are also available, and show slight changes in C_{lmax} (Pierce, 1947), however these were for 2-D foils, and do not include issues with the free surface or roughness. This project partially addresses that gap.
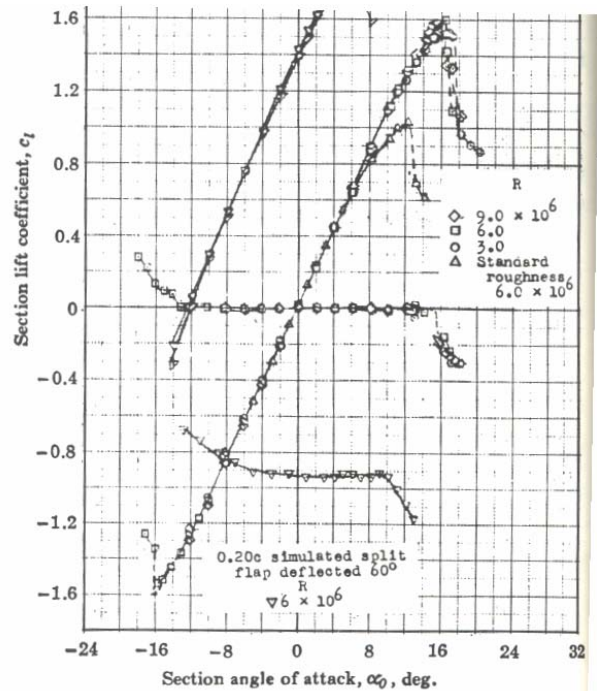

Figure 4: A plot showing the drop in C_{lmax} from approximately 1.6 to 1.0 due to roughness.

PHYSICAL ANALYSIS

As with most experiments, duplicating the actual in-service conditions was important to the accuracy of the results. Unfortunately we did not have access to a full-size yacht with the controlled environment to test it in! The initial project was intended to be conducted in the Naval

Academy's 380-foot tank and due to blockage effects we limited ourselves to a 16-foot, 1:5 scale model of an IACC yacht from the 1995 campaign of Team Dennis Conner. Hurricane Isabel intervened the week the tests were to start however, flooding our tank and destroying the equipment. Luckily our model floated with the flood waters and we were able to move to NSWC-CD to conduct our tests.

As we were researching hydrodynamic and fluid-structure effects, it was important to match as closely as possible the Froude and Reynold's numbers, as well as scaling the structural response. The model was ballasted to its designed waterline and a simple trapezoidal keel was installed to ensure keel wake effects were included. The model was towed at corresponding Froude numbers to likely in-service conditions. Strips of sand were added to the model, keel and rudders to trip the flow at the appropriate points. Two 12% section rudders were built with the same surface areas and with aspect ratios (S/C_m) of 2.2 and 3.4. A 1-inch diameter 6061-T6 aluminum rod was used as the rudder shaft. The skins were three plies of 4 oz E-glass cloth with ProSet epoxy. To minimize tripping effects, Paul Bogataj designed a section similar to a NACA 0012 that was relatively insensitive to the transition from laminar to turbulent flow across the angle of attack range. Figure 5 shows the model.
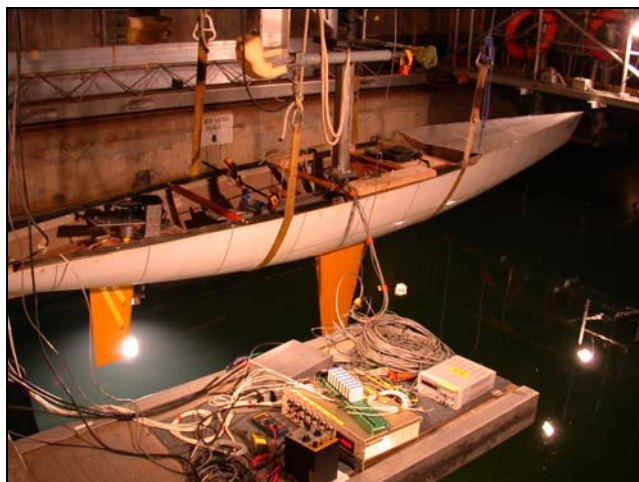

Figure 5: Model with low aspect ratio rudder

Each rudder was instrumented with eight, 0.5", 350-ohm, resistance strain gauges and the model was instrumented to record side force, yaw moment, pitch, heave, roll, rudder angle, velocity, and wave height. Prior to, and after the tank tests, each rudder was bench tested in water to establish or confirm baseline force versus strain data and watertight integrity of the strain gauges. The strain gauges were symmetrically placed on the rudders and were mounted: just above the lower rudder bearing, at 6 inch span, at 12 inch span and in a rosette at the middle of the shaft to measure torque. To avoid temperature issues the model was in the water a minimum of 30 minutes before the first data runs were taken.

The bench testing consisted of mounting each rudder in supports duplicating the rudder bearings and using weights to duplicate the anticipated static loads. The first goal of this bench test was to ensure that the gauges worked reliably underwater, which was not as easy as expected! Various techniques were used, with the best results obtained by "painting" the mounted gauges and wires with marine silicone sealant. The rudders remained underwater overnight in each test. Figure 6 shows the bench test. The block of wood was carved to match the rudder shape and the weights were placed on the wood. These controlled tests were checked against FEA runs to make sure the basic approach was correct before heading to the tank.

Figure 6: Static bench test of rudder strain gauges

A challenge existed in determining the actual location of the center of effort of the rudder. As mentioned earlier, a common assumption is that the center of effort is located at the centroid. Numerous studies have shown that this is reasonably accurate for design purposes, but would not be sufficiently accurate for this research project. The solution used a combination of CFD and model testing. The CFD will be explained below. The bench test gave us confidence that the FEA model could accurately match bending moment to strains observed in the shaft. As the moment is a linear combination of the center of effort's distance from the lower rudder bearing and the side force at the shaft, by isolating the side force and knowing the bending moment we could estimate the center of effort. We did this by using a force block attached to the model at the rudder location. This force block effectively measured yaw moment, and by varying the model's angle of attack we were able to isolate the rudder side force.

The testing goal was to capture the peak strains in the rudder shaft and correlate that to the vessel motions. As these are rapidly transient, an initial test run compared various sampling rates. This indicated 300 Hz would give sufficient resolution.

The basic test matrix for each rudder is shown in Table 1. This included both rudders running at speeds

corresponding to speed/length ratios (SLR) of 0.81 and 1.34. As we had only four days available to run the tank tests, we had to maximize our efficiency in the tank. Each run was roughly 3000 feet and required a 15 minute break to allow the tank to settle. To get as many data points as possible the rudders were servo controlled and could be thrown "hard over" numerous times on each run, with at least three different rudder rates used for each case. The angular velocity of the model rudder was programmed to be time-scaled to full-scale rudder movement. A shock absorber limited the model to approximately 10 degrees yaw and the rudder angle range was 0 to 32 degrees. In addition, as fixing the model in roll could impose artificially high loads, in Cases 5 and 8 the roll was free but roll damping springs were included. In Case 2, 3 and 6 the model was fixed in the upright condition.

Testing Matrix	
Case 1:	Fixed 0 Degrees Yaw / Free Roll
Case 2:	Fixed 0 Yaw / Fixed Roll
Case 3:	Fixed 5 Yaw / Fixed Roll
Case 4:	Fixed 5 Yaw / Free Roll
Case 5:	Free Yaw / Roll Damping
Case 6:	Free Yaw / Fixed Roll
Case 7:	Free Yaw / Free Roll
Case 8:	Low AR Rudder in Waves (Case 5 cond)

Table 1: Tank testing matrix

Four hundred and thirteen data sets were taken during the 33 runs comprising the eight (x 4) cases, but unfortunately we ran out of time for Case 9, which would have been the high aspect ratio rudder in waves. In addition, a planned series of tests at a SLR of 1.7 had to be cancelled due to fears of exceeding the dynamometer's capacity. The maximum wave height was set to 1-inch below the maximum freeboard of the model and the wave period was then set by the parameters of the JONSWOP shallow water spectrum as this gave the steepest waves.

NUMERICAL ANALYSIS

As mentioned earlier, one of the largest uncertainties was determining the center of effort, or more precisely, the center of pressure. This point moves with angle of attack, submergence and heel angle, and the traditional approach, while very useful for design purposes, was felt to be too inaccurate for this research project. Ideally a full 3-D viscous code with free surface effects would be used, however one was not available. The final approach used a combination of 2-D and 3-D CFD to approximate a pressure distribution near stall that could be mapped to the FEA models.

Three different CFD codes were used: X-foil,

PANAIR and SPLASH. X-foil, a 2-D viscous code, was used to estimate the chord-wise pressure distribution on the high and low pressure sides of the rudder near stall. PANAIR, a 3-D inviscid code was used to predict the spanwise pressure distribution on each side of the rudder. PANAIR is a fully-submerged code however and questions existed over what the free surface effects might have near the top of the rudder. In a static rest condition the top of the rudder was approximately 0.75" below the free surface. When heeled to approximately 15 degrees the top of the rudder was at the free surface when at rest. SPLASH, a 3-D inviscid code, was used to predict the free surface effects. Unfortunately the resolution on SPLASH was not as good as PANAIR, so a combined result was developed.

The three pressure distributions were then compared and a resulting pressure distribution was created for each rudder and Case. Figure 7 shows a typical chordwise pressure distribution profile from X-foil and Figure 8 shows the spanwise prediction from PANAIR. Figure 9 shows the resulting spanwise pressure distribution profile created by combining the PANAIR and SPLASH results. The influence on the center of effort location is clear.
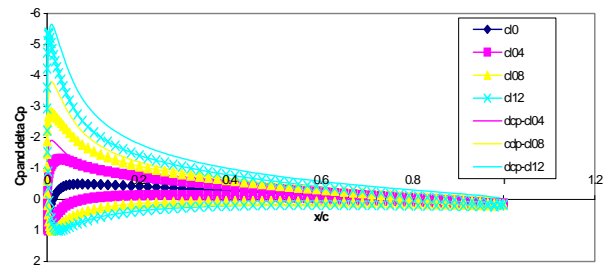

Figure 7: Non-dimensional chord wise pressure distribution from X-foil at C_L 0.4, 0.8, 1.2
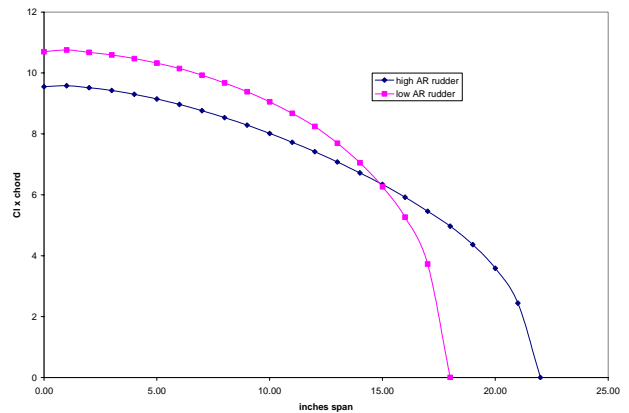

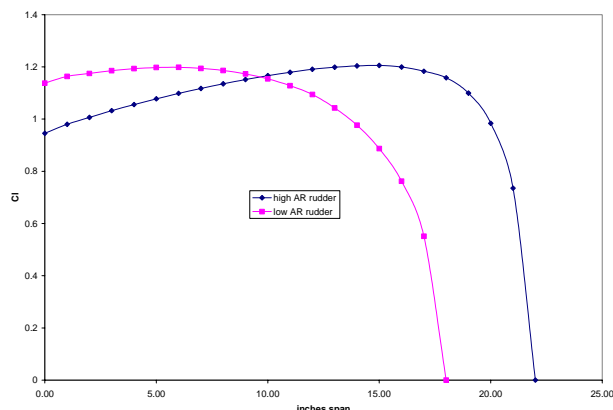Figure 8: Span wise distribution based on PANAIR for the rudders

Figure 9: Resulting spanwise pressure distribution from PANAIR and SPLASH results

The chord and span distributions were then used to create a 3-D pressure map for each side of each rudder. This pressure map was then used as the loading input for the finite element model.

FEA models of each rudder were constructed using the COSMOS/M program. Both rudders were built using solid elements to represent the core and stock and laminated shell elements for the skins. The models were initially checked against the static bench tests and deflections were within 2% of the predicted values. Strains at the three gauges (1" above the root, 6" and 12" below the root) agreed within 5%.

Not surprisingly, a basic check of whether the predicted side force from the CFD-derived model matched that from a steady state tank run, indicated some variation. In general the actual side force was 5-10% different than that predicted from the CFD. To calibrate the FEA model the pressures on the maps were uniformly scaled while keeping the relative distributions constant.

Figure 10 shows the exaggerated, deflected plot of the predicted strains from the FEA for the high aspect ratio rudder at its highest speed and observed loading. The highest strains are located where the strain gauge was located on the shaft. Note that the highest strains in the solid shaft, 0.0011, are approximately 27% of the yield strength of the 6061-T6 aluminum shaft. This is noteworthy in that it is well above the fatigue endurance limit for this material.
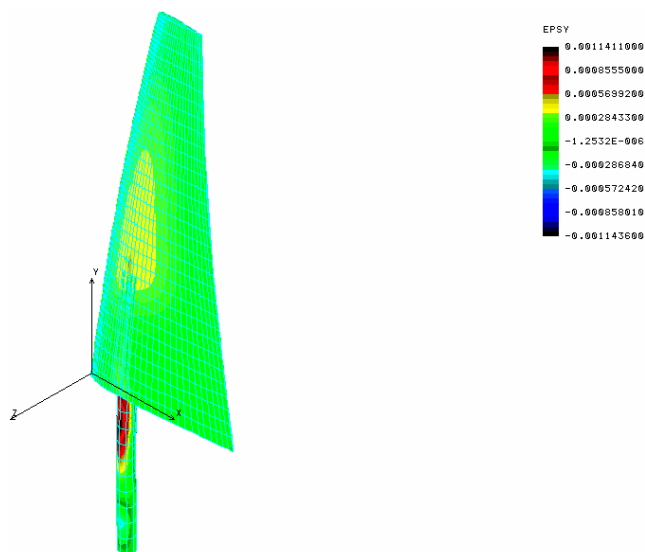

Figure 10: Predicted strain plot for high aspect ratio rudder at high speed

EXPERIMENTAL DATA

The eight cases from Table 1 were run for the two rudders and the two speeds. Prior to running Case 1 for each rudder, a benchmark "quasi-static" (i.e. a steady-state) test was performed where the model was run down the tank and the rudder was slowly rotated through the full angle of attack range to find the peak lift values. For the high aspect ratio rudder this generated a $C_L = 0.58$ for the slower speed and 0.57 for the higher speed, with the maximums reached at a consistent angle of attack of 14 degrees. For the low aspect ratio rudder the maximum C_L were 0.68 and 0.76 respectively, at an angle of attack of 19 degrees.

Figures 11-14 show the rudder angle, side force, roll angle and strain for a typical data set. The force and strain plots show a secondary peak shortly after the first. Correlating this to the roll angle plot and the high speed video indicate that the second peak occurred after the model had rebounded from the yaw limiter.

Of the 413 data sets taken, 302 yielded enough information to produce quantifiable results. The common problems were balky strain gage readings, fluctuations in the power supplies, rudder shaft slippage, and rudder shaft motor control issues where the shaft did not turn at a constant rate. Each condition was randomly repeated at least three times and the results were compared. In general the repeated tests showed that all the peak strains were within 10% and the majority of the times were within 5%. Interestingly, the range of rudder turn rates showed little variation in the results.
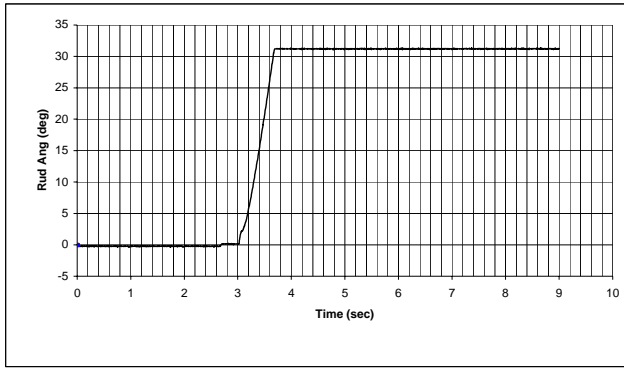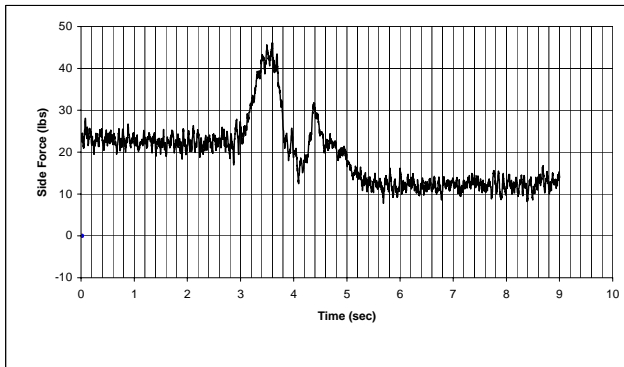
Figure 11: Rudder angle versus time

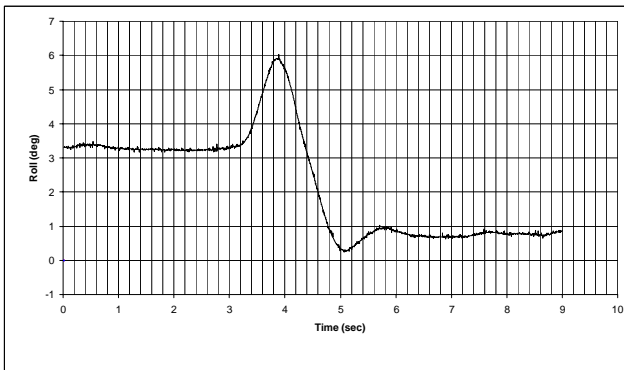Figure 12: Side force versus time

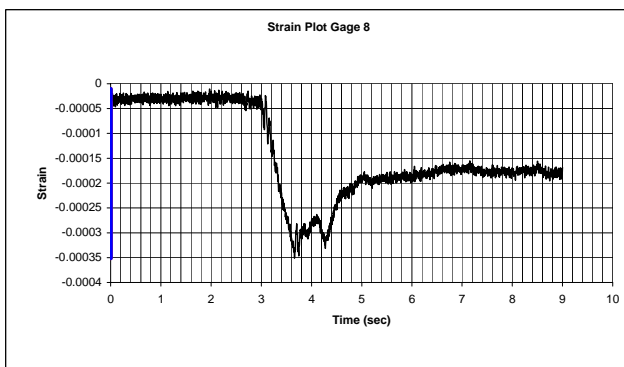Figure 13: Roll angle versus time

Figure 14: Strain versus time from shaft axial strain gauge

DISCUSSION

The first seven cases were based on different levels of model fixity. In reality a vessel is not constrained as much as a model, and the thought was that having greater constraints on the model would produce higher rudder loads and thus the actual loads on a real rudder would be less than those on a model rudder. This was borne out in the results. Figures 15 and 16 show the relative loading compared to Case 3, which was fully fixed at 5° yaw and 0° roll. The results are averaged for the low and high aspect ratio rudders except for Case 8, which is for the low AR rudder only. In general the lower SLR showed more uniform rudder loading. This makes sense as the higher speeds yielded faster reaction rates, which allowed for quicker load shedding. In addition, the rudders often ventilated during the higher speed runs. This would quickly reduce the rudder loading.

The largest reduction in loading was in the condition where the vessel was free to yaw and had some roll damping. In this case (#5) the load reduction ranged from 24-29%. The damping factor in Case 5 was calculated to approximate the aero damping of the rig and therefore this case might best represent reality. That the case (#7) where the vessel was fully free to respond did not have the greatest reduction may have been due to the very rapid response of the model, which almost immediately hit the roll limit and yaw damper. This is when the peak strain was taken as the strains continually increased to that point.
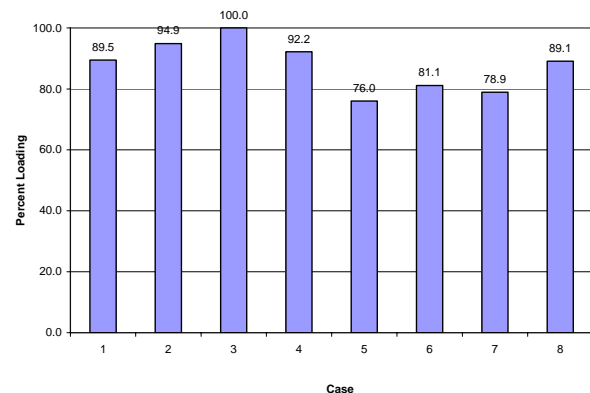

Figure 15: Relative maximum side force as a function of fixity for SLR = 0.81
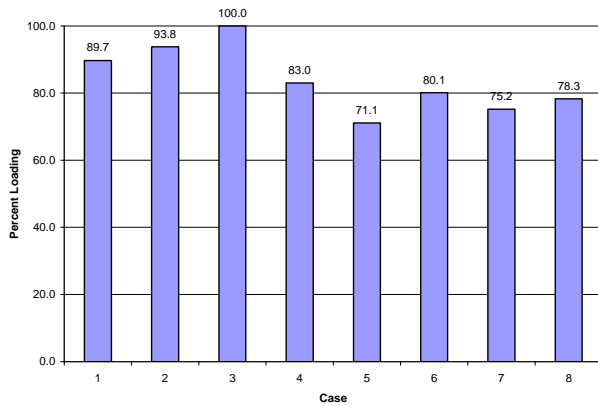
Figure 16: Relative maximum side forces as a function of fixity for SLR = 1.34.

Although the two figures do not show it, the difference in loading of the low aspect ratio rudder in waves was noticeable. Case 8 added waves to the Case 5 conditions of free to yaw and roll damping. Understandably, the data from these runs were quite scattered and were heavily influenced by the particular pitch condition when the rudder was turned. If the turn started at the same time the bow was rising, the increase in loading was 16% for the low speed case and 10% for the high speed case. These values were derived from only one data set however and should not be taken as conclusive.

After the loads were converted into the pressure maps and the FEA correlated to the strains, the final step was to back out the lift coefficients based on the center of effort location equal to the centroid, as is done in the ABS calculations. Table 2 shows the peak rudder coefficients using this method. It is apparent that the ABS value of 1.5 was only matched in the most constrained condition, and at the slower speed. The most realistic conditions, Cases 5 and 8, showed significantly lower lift coefficients. Note that all of these dynamic coefficients are significantly larger than the quasi-static coefficients found during the steady state conditions.

	Low AR SLR=0.81	Low AR SLR=1.34	High AR SLR=0.81	High AR SLR=1.34
Case 1	1.37	1.17	1.38	1.24
Case 2	1.46	1.22	1.46	1.29
Case 3	1.53	1.30	1.54	1.38
Case 4	1.41	1.08	1.42	1.14
Case 5	1.17	0.93	1.17	0.98
Case 6	1.24	1.04	1.25	1.10
Case 7	1.21	0.98	1.21	1.04
Case 8	1.36	1.02		
Steady-State	0.68	0.78	0.58	0.57

Table 2: Maximum rudder lift coefficients for various constraint conditions based on CE at centroid

CONCLUSIONS

This study illustrated a number of important relationships in rudder structural design, in particular that maximum lift coefficients increase in dynamic conditions, and that the more relaxed rigid body constraints in service do lower the load compared to model results. Aspect ratios within the ranges tested appeared to have little impact on the maximum lift coefficients, but ventilation can have a significant affect.

In regards to the simplified method used by ABS, it appears 10-15% conservative when taken as a single event. In cases of materials where the fatigue limit is relatively low, such as many aluminum alloys, the ABS approach may not give adequate margin for long-term service.

Future work should address a number of questions raised in this project. First would be to quantify the effect of the sand strips versus a polished rudder, one with Hama Strips and one with normal bottom paint. They were added to avoid laminar separation issues but may have affected the maximum lift coefficients observed. The impact of waves was barely touched. A very worthwhile experiment would be to compare the dynamic effects of the vessel heeled in waves where the rudder would see increased span flow and potentially higher bending moments. Of course, the best test would be to strain gauge a modern sailing yacht's rudder and record the data over a long period of time.

ACKNOWLEDGEMENTS

REFERENCES

Abbott, I. H., and Von Doenhoff, A. E., "Theory of Wing Sections", Dover Publications, New York, 1959

American Bureau of Shipping, "Guide for Building and

Classing Offshore Racing Yachts", 1994/1997

Bea, R. G., "Design Criteria for Marine Structures", notes from a graduate course at U. C. Berkeley, NA290C, Spring 1993

Lewandowski, E. M., "The Effects of Reynolds Number, Section Shape, and Turbulence Stimulation on the Lift of a Series of Model Control Surfaces", Proceedings of the 22nd American Towing Tank Conference, 1989.

Marchaj, C. A., "Aero-Hydrodynamics of Sailing", Dodd, Mead and Company, New York, 1979

Miller, P. H., "Design Criteria for Composite Masts," 12th CSYS, 1995

Patton, J. R., "Evaluation of Dynamic Lift Coefficients of High Aspect Ratio Rudders and Control Surfaces", Trident Scholar project report no. 325, United States Naval Academy, 2004

Pierce, H., "On the Dynamic response of Airplane Wings Due to Gusts", NACA TN No. 1320, 1947

Silverberg, J. P., "Performance Prediction of the Mk II Navy 44 Sail Training Craft with respect to Tank Testing, Velocity Prediction Programs, and Computational Fluid Dynamics", Trident Scholar project report no. 315, United States Naval Academy, 2003